Heliyon 10 (2024) e36064

Contents lists available at ScienceDirect

Heliyon

journal homepage: www.cell.com/heliyon

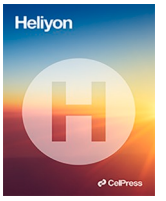

Research article

Exploring thermophysical properties of CoCrFeNiCu high entropy alloy via molecular dynamics simulations

Fan Liu [a], Yuqing Liu [a], Xi Zhuo Jiang [a,*], Jun Xia [b,c]

[a] School of Mechanical Engineering and Automation, Northeastern University, Shenyang, Liaoning, 110819, China
[b] Department of Mechanical and Aerospace Engineering, Brunel University London, Uxbridge, UB8 3PH, United Kingdom
[c] Institute of Energy Futures, Brunel University London, Uxbridge, UB8 3PH, United Kingdom

ARTICLE INFO

Keywords:
High entropy alloy
Molecular dynamics
Lattice thermal conductivity
Volumetric specific heat capacity
Phonon density of states
Phonon mean free path

ABSTRACT

High entropy alloys (HEAs) are alloys composed of five or more primary elements in equal or nearly equal proportions of atoms. In the present study, the thermophysical properties of the CoCrFeNiCu high entropy alloy (HEA) were investigated by a molecular dynamics (MD) method at nanoscale. The effects of the content of individual elements on lattice thermal conductivity k_p were revealed, and the results suggested that adjusting the atomic content can be a way to control the lattice thermal conductivity of HEAs. The effects of temperature on k_p were investigated quantitively, and a power-law relationship of k_p with $T^{-0.419}$ was suggested, which agrees with previous findings. The effects of temperature and the content of individual elements on volumetric specific heat capacity C_v were also studied: as the temperature increases, the C_v of all HEAs slightly decreases and then increases. The effects of atomic content on C_v varied with the comprising elements. To further understand heat transfer mechanisms in the HEAs, the phonon density of states (PDOS) at different temperatures and varying atomic composition was calculated: Co and Ni elements facilitate the high-frequency vibration of phonons and the Cu environment weakens the heat transfer via low-frequency vibration of photons. As the temperature increases, the phonon mean free path (MFP) in the equiatomic CoCrFeNiCu HEA decreases, which may be attributed to the accelerated momentum of atoms and intensified collisions of phonons. The present research provides theoretical foundations for alloy design and have implications for high-performance alloy smelting.

1. Introduction

High entropy alloys (HEAs) are alloys composed of five or more primary elements in equal or nearly equal atomic proportions, and every individual element accounts for 5 %–35 % in terms of the atomic content [1]. Such atomic ratio hinders the generation of intermetallic compounds or complex phases in the alloy and instead favours the formation of simple solid solution phases [2,3], such as face-centered cubic (FCC), body-centered cubic (BCC) and hexagonal close-packed (HCP) structures. HEAs exhibit four distinctive core effects: the high configurational entropy effect, the lattice distortion effect, the slow diffusion effect and the "cocktail" effect [4]. These core effects endow HEAs with exceptional mechanical strength and toughness [5,6], wear resistance [7–9], oxidation resistance [10], corrosion resistance [11,12] and unique thermal properties [12]. HEAs are widely applied to various fields, including mechanics,

* Corresponding author.
E-mail address: jiangxz@mail.neu.edu.cn (X.Z. Jiang).

https://doi.org/10.1016/j.heliyon.2024.e36064
Received 21 May 2024; Received in revised form 24 July 2024; Accepted 8 August 2024
Available online 9 August 2024

chemistry [13] and biology [14]. Popular HEAs include cantor HEAs (FeCoNiMnCr [15]), refractory alloys (VNbMoTaW [16]) and non-Cantor dual-phase alloys (e.g., AlCuSiZnFe [17]).

The term "high-entropy alloy" was introduced by Yeh et al. in 2004 [18,19]. The multiple principal elements in HEAs, especially those with significant atomic radius differences, cause lattice distortion [20]. The lattice distortion and inherent chemical disorder of HEAs lead to fluctuations in interatomic force constants and mass, resulting in intensified anharmonic phonon-phonon interactions [21] and a reduced lattice thermal conductivity. Studies have shown that HEAs exhibit semimetallic characteristics, where the contribution of phonons to heat conduction can be comparable to that of electrons [22]. Moreover, charge carriers can move freely when the phonons are hindered and scattered, which is beneficial for achieving a high ZT (thermoelectric figure of merit) value as well as a high efficiency in thermal-energy management [23]. These features suggest that HEAs are potential next-generation thermoelectric materials. Therefore, researching the thermal physical properties and heat transfer mechanisms of HEAs is of great significance. Over the past two decades, researchers have extensively studied the phase, microstructure and mechanical properties of the HEAs. Recently, studies about the thermophysical properties, like thermal conductivity, of HEAs have emerged. As summarised in Table 1, the thermal conductivity of HEAs is affected by a wide range of factors, including temperature, chemical composition and microstructure.

A molecular dynamics (MD) method is a powerful tool to reproduce the atomic events inside a system. By solving Newton's law of motion of the constituent atoms, MD is able to track the trajectories of all the atoms and molecules [29] and is thus widely used to interpret interesting phenomena in thermal [30–33], biological [34,35] and chemical reaction systems [36,37]. MD has also been used to understand the mechanisms for some unique behaviours of HEAs. For example, Caro et al. [20] used the MD method to identify the intermolecular interactions that could affect the thermal conductivity of HEA and thereby proposed the strategies to control the thermal conductivity. By using an MD method, Shi et al. [38] clarified that the $Al_{0.3}$CoCrFeNi HEA has significant semi-metallic features, and the heat conduction in such an HEA is mainly achieved by phonons. Such studies imply that MD could be an alternative but promising method to explore key features of the HEAs.

CoCrFeNiCu is a functional material that has the potential to be applied to harsh working conditions, like in the aerospace. To better understand the performance of such a material, the mechanical and thermophysical properties of the CoCrFeNiCu should be investigated. Previous studies have demonstrated that the CoCrFeNiCu HEA performs well in resisting radiation and bacteria [39–41]. However, the thermophysical properties of CoCrFeNiCu are unknown, and the lack of the thermophysical data may hinder the application of such an HEA to extreme conditions like high temperatures and high pressures.

In the present study, the thermophysical properties (thermal conductivity and volumetric specific heat capacity) of the CoCrFeNiCu HEA are systematically investigated via the MD method. A series of MD simulations are performed to explore the influencing factors (e.g., temperature and chemical composition) that may affect the thermal conductivity and the volumetric specific heat capacity of the CoCrFeNiCu HEA. Furthermore, phonon density of states (PDOS) analysis is conducted to understand how the influencing factors affect the heat transfer of HEAs. This research provides theoretical foundations for the design and optimisation of new HEA materials.

Table 1
Influencing factors of the thermal conductivity of HEAs from references.

Influencing factors	HEAs	Key findings	Ref.
Temperature	Al_xCoCrFeNi	Thermal conductivity increases with temperature.	[24]
	CrMnFeCoNi	The electrical and thermal conductivities are significantly reduced compared to Ni, and the temperature dependence of lattice thermal conductivity exhibits a glasslike plateau.	[25]
	Al_2CoCrFeNi	The thermal conductivity of the cast and annealed HEA increases with temperature.	[23]
Chemical composition	Al_xCoCrFeNi	Thermal conductivity decreases with x in the single-phase region and is lower than the most of the pure metals.	[26]
	CoCrFeNiNb_x	Thermal conductivity increases with x at low temperatures but decreases with x at high temperatures.	[27]
	$W_{60}Ta_{20}V_{20}$, WTaV, $W_{40}Ta_{20}V_{20}Ti_{20}$, WTaVTi, WTaVTiCr	The presence of Ta, Ti, V and Cr could alter the trend of thermal conductivity with temperature in W alloys.	[28]
	NiCoFe, NiCoMn, NiFeMn, NiCoFeMn, NiCoCr, NiCoFeCr, NiCoMnCr, NiCoFeMnCr, NiCoFeCrPd	The presence of Cr/Mn/Pd significantly decreases thermal conductivity.	[22]
Microstructure	Al_2CoCrFeNi	The microstructures of cast and annealed HEA differ. At 300–800 °C, the thermal conductivity of the cast HEA is higher than annealed HEA at 1300 °C, and the overall thermal conductivity of the annealed HEA at 1000 °C is the lowest.	[23]

2. Methods

2.1. Model construction and case set-ups

The Large-scale Atomic/Molecular Massively Parallel Simulator (LAMMPS) was employed to build the HEA model and conduct the subsequent calculation [42]. The simulation domain was a cuboid with the length (X direction) and breath (Y direction) of 50 Å, respectively, and a varying height (Z direction), l_z. The details of the initial structure can be found in the **Supplementary Materials**. Fig. 1 illustrates a typical initial configuration of the HEA model in the MD simulation.

To investigate the effects of chemical composition, size and temperature on the thermophysical properties of the CoCrFeNiCu HEA, 21 cases were set up as shown in Table 2.

Cases 1–10 were designed to investigate the influence of chemical composition, size and temperature on thermal conductivity k_p. Cases 11–15 were designed to study the effects of atomic content of different elements and temperature on volumetric specific heat capacity C_v. Cases 16–21 were designed to calculate phonon density of states with the atomic content of different elements and different temperatures.

2.2. Simulation details and data post-processing

The interactions between Co–Cr–Fe–Ni–Cu atoms were calculated using an Embedded Atom Method (EAM) potential [39,43] whose reliability had been confirmed in a previous study [44]. Indeed, the reliability of the EAM potential was also verified by the present study: the average lattice constant of equiatomic CoCrFeNiCu HEA under the EAM potential in the present study is 3.553 Å, which agrees with the lattice constants reported from experiments (3.54 Å) [45] and a density functional theory (DFT) study (3.56 Å) [46].

2.2.1. Construction of a metastable metallic structure

The HEA model was first energy-minimized at the target temperature. The structure was further relaxed in an NPT ensemble for 1 ns, and PBCs were applied to the X and Y directions and a shrink-wrapped boundary condition to the Z direction. After an additional 100-ps relaxation in an NVT ensemble, a metastable metallic structure of HEA was eventually formed. The details can be found in the **Supplementary Materials**.

2.2.2. Calculation of thermal conductivity

In the present study, a Non-Equilibrium Molecular Dynamics (NEMD) [47] simulation was used to simulate the heat transfer process. NEMD is an effective method for addressing heat and mass transfer problems, where the systems of interest are not in thermodynamic equilibrium.

A Langevin method (Fig. 2a) was used to calculate the thermal conductivity k. Fourier's Law of heat transfer then gives,

$$k = -\frac{J_z}{dT/dZ} \tag{1}$$

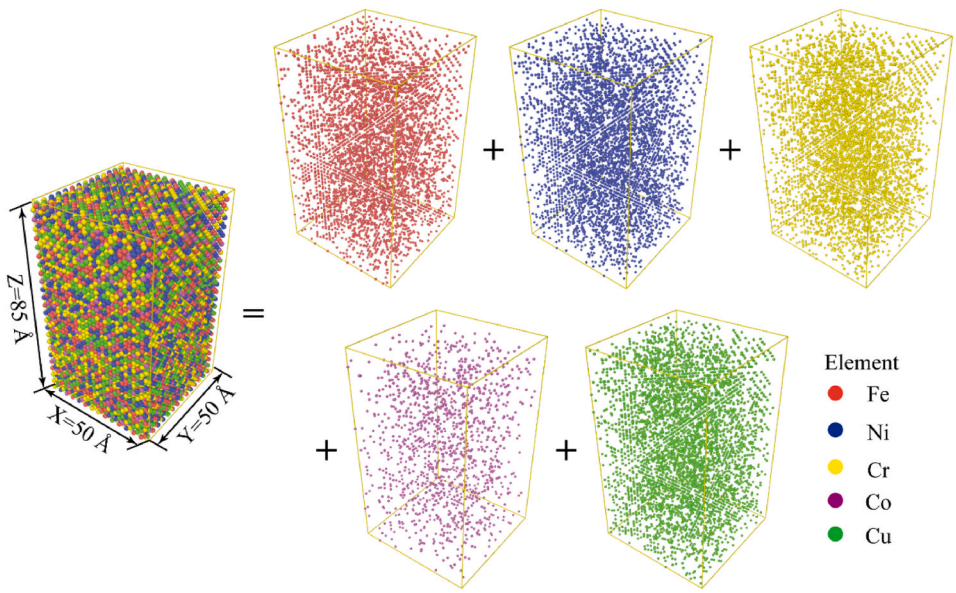

Fig. 1. A typical initial configuration of the CoCrFeNiCu HEA.

Table 2
Cases set-up in the present study.

Case	l_x, l_y, Å	l_z, Å	T, K	Number of atoms	Atomic ratio
1	50	80	300	18816	Co:Cr:Fe:Ni:Cu = x:1:1:1:1
2	50	80	300	18816	Co:Cr:Fe:Ni:Cu = 1:x:1:1:1
3	50	80	300	18816	Co:Cr:Fe:Ni:Cu = 1:1: x:1:1
4	50	80	300	18816	Co:Cr:Fe:Ni:Cu = 1:1:1: x:1
5	50	80	300	18816	Co:Cr:Fe:Ni:Cu = 1:1:1:1:x
6	50	60	300~1100	14112	Co:Cr:Fe:Ni:Cu = 1:1:1:1:1
7	50	80	300~1100	18816	Co:Cr:Fe:Ni:Cu = 1:1:1:1:1
8	50	100	300~1100	22736	Co:Cr:Fe:Ni:Cu = 1:1:1:1:1
9	50	150	300~1100	33712	Co:Cr:Fe:Ni:Cu = 1:1:1:1:1
10	50	200	300~1100	45080	Co:Cr:Fe:Ni:Cu = 1:1:1:1:1
11	50	50	300~1100	10976	Co:Cr:Fe:Ni:Cu = x:1:1:1:1
12	50	50	300~1100	10976	Co:Cr:Fe:Ni:Cu = 1:x:1:1:1
13	50	50	300~1100	10976	Co:Cr:Fe:Ni:Cu = 1:1: x:1:1
14	50	50	300~1100	10976	Co:Cr:Fe:Ni:Cu = 1:1:1: x:1
15	50	50	300~1100	10976	Co:Cr:Fe:Ni:Cu = 1:1:1:1:x
16	50	50	300	10976	Co:Cr:Fe:Ni:Cu = x:1:1:1:1
17	50	50	300	10976	Co:Cr:Fe:Ni:Cu = 1:x:1:1:1
18	50	50	300	10976	Co:Cr:Fe:Ni:Cu = 1:1: x:1:1
19	50	50	300	10976	Co:Cr:Fe:Ni:Cu = 1:1:1: x:1
20	50	50	300	10976	Co:Cr:Fe:Ni:Cu = 1:1:1:1:x
21	50	50	300~1100	10976	Co:Cr:Fe:Ni:Cu = 1:1:1:1:1

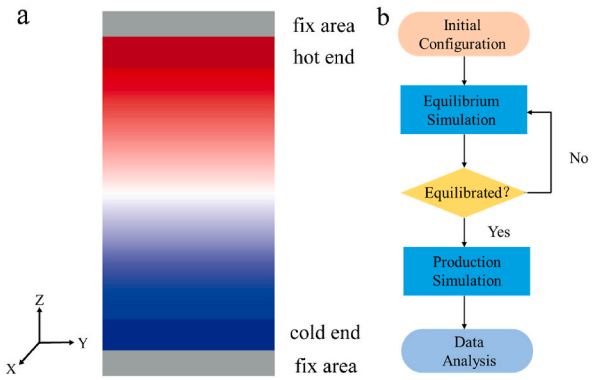

Fig. 2. Model and simulation flowchart. a. A Langevin model for calculating the thermal conductivity in an NEMD simulation. b. Flowchart for MD simulation in the present study.

where Z is the direction of heat transfer (Fig. 2), J_z is the heat flux between the hot and cold ends in the Z direction, and dT/dZ is the temperature gradient generated.

The calculation details of the thermal conductivity can be found in the **Supplementary Materials**.

2.2.3. Calculation of volumetric specific heat capacity

The volumetric specific heat was calculated by Eq. (2) [48]:

$$C_v = \frac{(\partial E/\partial T)_V}{V} \tag{2}$$

where C_v is the volumetric specific heat capacity, E is the total energy, T is the temperature, and V is volume.

The calculation details of volumetric specific heat capacity capacity can be found in the **Supplementary Materials**. The simulation flowchart for calculating thermal conductivity and volumetric specific heat capacity is shown in Fig. 2b.

2.2.4. Calculation of photon density of states

The phonon density of states in a material system gives the number of phonon states that can be occupied at a certain level of frequency or energy, providing insights into atomic activity in materials. The Fourier Transform of the atomic velocity auto-correlation function (VACF) obtained from MD simulations was used to calculate PDOS. The formulas are as follows [30,49]:

$$F(\omega) = \sum_{\alpha} F_{\alpha}(\omega) \tag{3}$$

$$F_\alpha(\omega) = \int \frac{\langle V_{i\alpha}(0) \cdot V_{i\alpha}(t) \rangle}{\langle V_{i\alpha}(0) \cdot V_{i\alpha}(0) \rangle} e^{-2\pi i\omega t} dt \quad (4)$$

where ω represents the vibration frequency of phonon, $F_\alpha(\omega)$ denotes the partial PDOS, and $V_{i\alpha}$(t) and $V_{i\alpha}$(0) denote the velocities of the ith particle of species α at time t and time 0, respectively. The bracket refers to the average of the atomic and temporal origins.

2.2.5. Statistics

For cases 1–15, five replicates with different initial configurations were simulated. For cases 16–21, three replicates with different initial configurations were simulated. Unless otherwise indicated, data with error bars represent mean ± SD (standard deviations).

3. Results and discussion

Thermal conductivity and specific heat capacity are two widely used thermophysical properties in heat transfer process. Herein, the influencing factors of the thermal conductivity and specific heat capacity for HEAs are discussed in detail.

3.1. Lattice thermal conductivity

The thermal conductivity k of a material consists of the electronic thermal conductivity and the lattice thermal conductivity k_p. As the outputs of MD simulation are mainly atomic trajectories, the thermal conductivity discussed in this paper is the lattice thermal conductivity. The effects of chemical composition in terms of content of the constituent atoms, size of the HEA and temperature on the lattice thermal conductivity of the CoCrFeNiCu HEA are investigated.

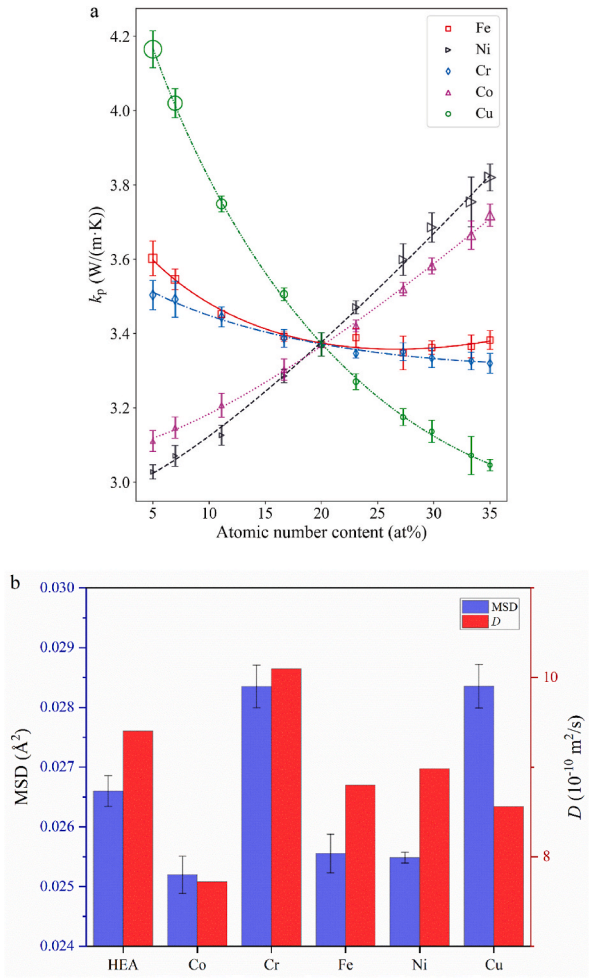

Fig. 3. The lattice thermal conductivity k_p, MSD and diffusion coefficients of the CoCrFeNiCu HEAs. a. Changes of lattice thermal conductivity k_p with the atomic content of five constituent elements. b. MSD and atomic diffusion coefficients of the CoCrFeNiCu HEA and the individual constituent elements.

3.1.1. Effects of chemical composition on k_p

Cases 1 to 5 in Table 2 were conducted to investigate the effects of chemical composition on k_p. The chemical composition was changed by varying the atomic number content of individual elements of the HEA from 5 at% to 35 at% at 300 K, and the corresponding subscripts x for the HEA chemical formulas $Co_xCrFeNiCu$, $CoCr_xFeNiCu$, $CoCrFe_xNiCu$, $CoCrFeNi_xCu$ and $CoCrFeNiCu_x$ varied from 0.211 to 2.15.

Fig. 3a shows the changes in lattice thermal conductivity k_p with the atomic number content of individual elements. The effects of chemical composition on k_p are manifold: Cr and Fe elements slightly decrease k_p. Co and Ni elements enhance lattice thermal conduction as the atomic contents increase; by contrast, Cu hinders lattice thermal conduction as the atomic content increases. The slight increase in k_p at 23 at% Fe content may be due to fluctuations of statistics.

According to the research of Caro et al. [20] and Chou et al. [26], both atomic radius and atomic mass in HEA affected the lattice thermal conductivity. The incorporation of larger-sized atoms into the lattice of smaller-sized atoms resulted in lattice distortion, which reduced lattice thermal conductivity. Herein, the average atomic radius of the Co, Cr, Fe, Ni and Cu atoms is 1.266 Å. Cr (1.28 Å) and Fe (1.27 Å) atoms have slightly larger atomic radius than the average, and an insignificant decrease in k_p was observed. Cu (1.28 Å) has larger atomic radius and atomic mass which contribute to the decrease of k_p as the atomic content increases. The atomic radii of Co (1.25 Å) and Ni (1.25 Å) are smaller the average radius of the HEA, and an increase in k_p can be expected.

Fig. 3a further suggests that adjusting the atomic content of the constituent elements could be a way to control the lattice thermal conductivity of HEA. Such findings will have potential for significantly reducing metallurgical costs. For example, HEAs with 20 at% of Co atoms and 35 at% of Fe atoms can both achieve the thermal conductivity of 3.4 W/(m·K). The cost of HEAs with 35 at% Fe atoms is expected to be lower than those with 20 at% Co atoms, as the Fe element has lower mining and smelting costs than those of the Co element.

The addition of element could also cause lattice structure and atomic behaviour changes. Herein, the lattice distortion of the HEA and individual atoms were calculated in terms of mean-square-deviations (MSD) of atoms [50,51] (Details can be found in the **Supplementary Materials**). Also, the atomic behaviour changes were evaluated in terms of the atomic diffusion coefficients (D). Fig. 3b compares the MSD and atomic diffusion coefficients among the HEA and individual comprising elements. As shown in Fig. 3b, the addition of Cr and Cu atoms could cause severe lattice distortion, whilst the influences of Co, Fe and Ni on lattice distortion are moderate. The addition of Cr could benefit the atomic diffusion, while Co, Fe, Ni and Cu could hinder atomic diffusions.

3.1.2. Effects of HEA size on k_p

The simulated system investigated by MD is nanoscale, which the phonon mean free path (MFP) $l_{p,}$ is close to the characteristic length, and the effects of the HEA size on k_p should not be neglected. This section takes the equiatomic CoCrFeNiCu HEA as an example, and the effects of HEA size on k_p is discussed (cases 6–10). The length (x-direction) and width (y-direction) of the simulation domain is 50 Å; by varying the height (z-direction, l_z) the HEA size is modified from 60 to 200 Å.

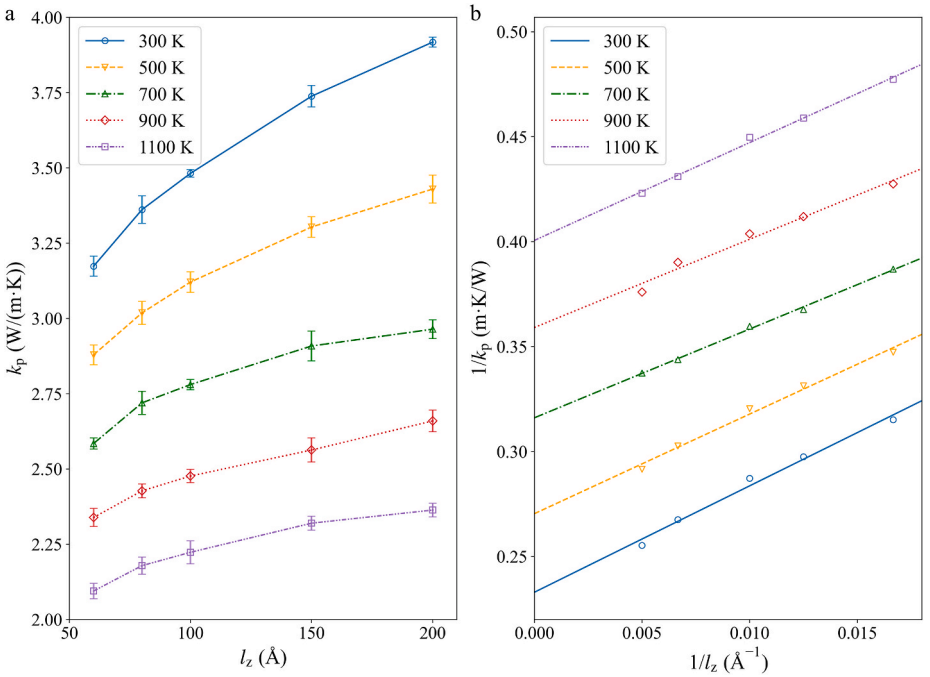

Fig. 4. Effects of the HEA size on the lattice thermal conductivity. a. The lattice thermal conductivity k_p changes with the HEA size at 300 K, 500 K, 700 K, 900 K and 1100 K. b. The fitting curve of $1/k_p$ and $1/l_z$ to calculate the lattice thermal conductivity after eliminating the size effect.

Fig. 4a shows the change of the lattice thermal conductivity k_p with different HEA sizes at varying temperatures, and k_p increases with the HEA size at all temperatures involved. The slope of the k_p-l_z curve decreases as the HEA size increases. The size effect on k_p can be eliminated as the simulation domain approach macroscale. The corrected thermal conductivity after eliminating the size effect is determined by the inverse of the ordinate intercept of the $1/k_p$-$1/l_z$ fitting curve [52,53] in Fig. 4b. The corrected lattice thermal conductivity k_p after eliminating the size effect is provided in Table 3.

3.1.3. Effects of temperature on k_p

Fig. 5 shows the lattice thermal conductivity k_p of bulk equiatomic CoCrFeNiCu HEA after eliminating the size effect as a function of temperature in double logarithmic coordinates, and k_p decreases with the increase of temperature. A power law distribution can be applied to the relationship between k_p and T with the law's exponent of −0.419 (i.e., $k_p \sim T^{-0.419}$), which agrees with a previous study [38].

3.2. Volumetric specific heat capacity

Cases 11–15 were conducted to study the effects of atomic content of different elements and temperature on volumetric specific heat capacity C_v. $CoCrFe_xNiCu$, $CoCrFeNi_xCu$, $CoCr_xFeNiCu$, $Co_xCrFeNiCu$ and $CoCrFeNiCu_x$ ($x = 0.21$, 0.5, 1, 1.5 and 2.15) HEAs with dimensions of 50 Å × 50 Å × 50 Å were used to calculate the C_v.

Fig. 6 manifests the volumetric specific heat capacity C_v of the $CoCrFe_xNiCu$, $CoCrFeNi_xCu$, $CoCr_xFeNiCu$, $Co_xCrFeNiCu$ and $CoCrFeNiCu_x$ ($x = 0.21$, 0.5, 1, 1.5 and 2.15) HEAs with different element atomic content at 300 K–1100 K. As the temperature increases, the volumetric specific heat capacity C_v of all HEAs slightly decreases and then increases. A similar trend was also reported in a previous study about the $Al_{0.3}CoCrFeNi$ HEA [38]. As the temperature rises to around 450 K, the interatomic motion barrier is broken by the thermal activation, allowing the HEA to gradually transit to a steady state, and atoms are locally ordered in the short range. The short-range ordered distribution of atoms means a reduced number of phonon modes, which accounts for the decrease in C_v. As the temperature continues to rise, the material undergoes an order-to-disorder transition. At such point, due to the increase in entropy, additional heat is absorbed by the HEA and C_v increases.

The effects of atomic content on C_v vary with the elements: the addition of Fe and Cu leads to the reduction in C_v; by contrast, the addition of Ni, Cr and Co increases the C_v of the HEA. Co and Cr elements have the least impact on C_v (3470–3540 kJ/(m^3·K)), the effects of Fe and Ni elements on C_v are significant (3450–3570 kJ/(m^3·K)), and the influence of Cu element is relatively moderate (3455–3550 kJ/(m^3·K)).

3.3. Phonon density of states

3.3.1. Effects of element atomic content on PDOS

To further understand the physical mechanisms underlying the change on the thermal conductivity of HEAs by the atomic content of different elements, the phonon density of states was calculated (cases 16–20). The velocities of atoms were correlated every 5 fs for a total integration time of 20 ps.

A probability density function was used to illustrate the PDOS distribution with vibration frequency, as shown in Fig. 7a to e. To further identify the trend in individual figures, a cumulative distribution function was adopted. The cumulative phonon density of States (CPDOS) was calculated by the integral probability of the phonons with the vibration frequency spreading from 0 to ω, as shown in Fig. 7f to j.

The PDOS are almost in the frequency range less than 12.5 THz, which agrees with previous calculations by Lokman Ali et al. [54]. In Fig. 7a to e, the PDOS has two peaks: the first peak almost overlaps as the atomic content varies, while the second peak, in the high-frequency region, is either enhanced or diminished, thereby affecting the thermal conductivity. For $Co_xCrFeNiCu$ and $CoCrFeNi_xCu$, the peak of the PDOS shifts towards high-frequency region as the atomic content increases, suggesting that Co and Ni elements facilitate the high-frequency vibration of phonons. For the $CoCrFeNiCu_x$ HEA, as the atomic content of Cu increases, the peak of the PDOS shifts towards the low frequency region, manifesting the Cu environment weakens the heat transfer via low-frequency vibration of phonons. The low-frequency vibration of phonons further results in lower thermal conductivity values at higher Cu content [55].

3.3.2. Effects of temperature on PDOS for the equiatomic CoCrFeNiCu HEA

The PDOS of the equiatomic CoCrFeNiCu HEA was calculated for cases of different temperatures, as shown in Fig. 8. At all temperatures, most of the phonons (about 80 % as shown in Fig. 8b) vibrate with a frequency between 4.4 THz and 9.8 THz (Fig. 8a). The number of phonons vibrating at such a range increases as temperature decreases, accounting for the decreasing trend of k_p with increasing temperatures in Fig. 4a. High-frequency phonons (frequency >9.8 THz) are more likely to be observed in high temperature

Table 3
Corrected lattice thermal conductivity k_p after eliminating the size effect.

Temperature (K)	300	500	700	900	1100
intercept of the $1/k_p$-$1/l_z$ curve	0.2330	0.2704	0.3161	0.3591	0.4006
R^2 of the $1/k_p$-$1/l_z$ curve	0.9870	0.9895	0.9977	0.9770	0.9955
k_p (W/(m·K))	4.292	3.699	3.163	2.785	2.496

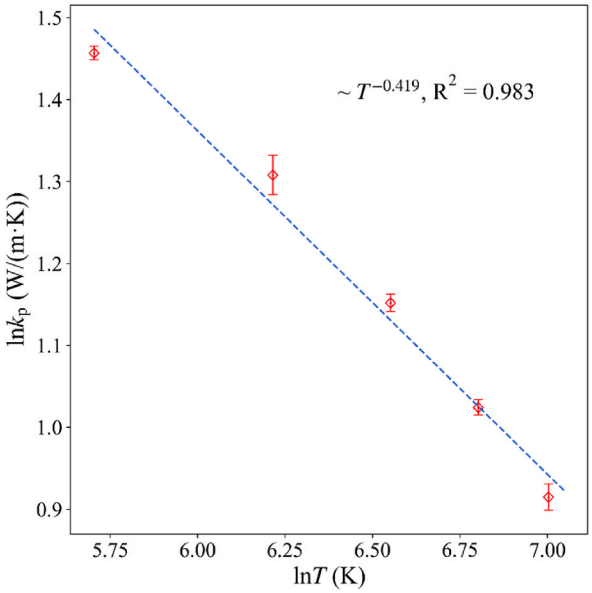

Fig. 5. The lattice thermal conductivity k_p of bulk equiatomic CoCrFeNiCu HEA after eliminating the size effect as a function of temperature illustrated in double logarithmic coordinates.

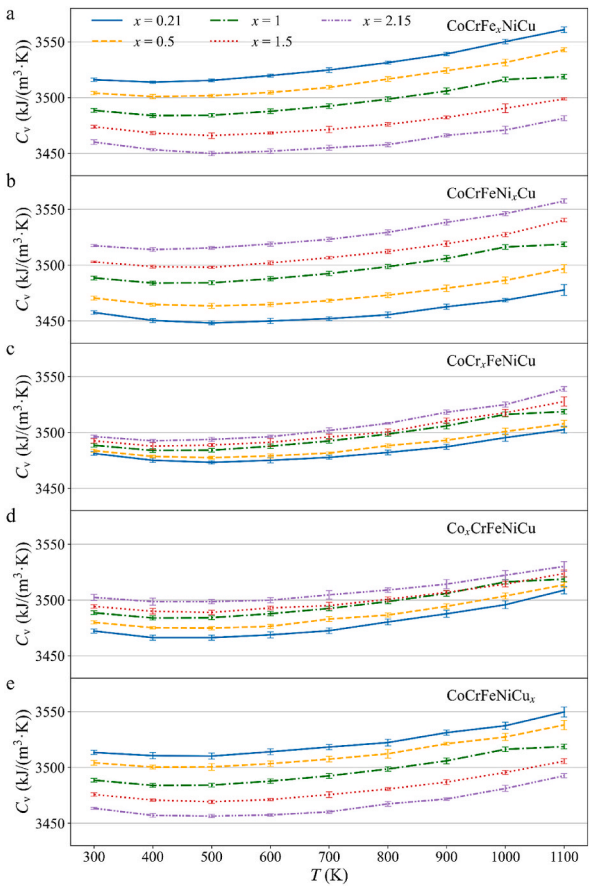

Fig. 6. The volumetric specific heat capacity C_v of the HEAs with varying element atomic content. a. CoCrFe$_x$NiCu, b. CoCrFeNi$_x$Cu, c. CoCr$_x$FeNiCu, d. Co$_x$CrFeNiCu and e. CoCrFeNiCu$_x$.

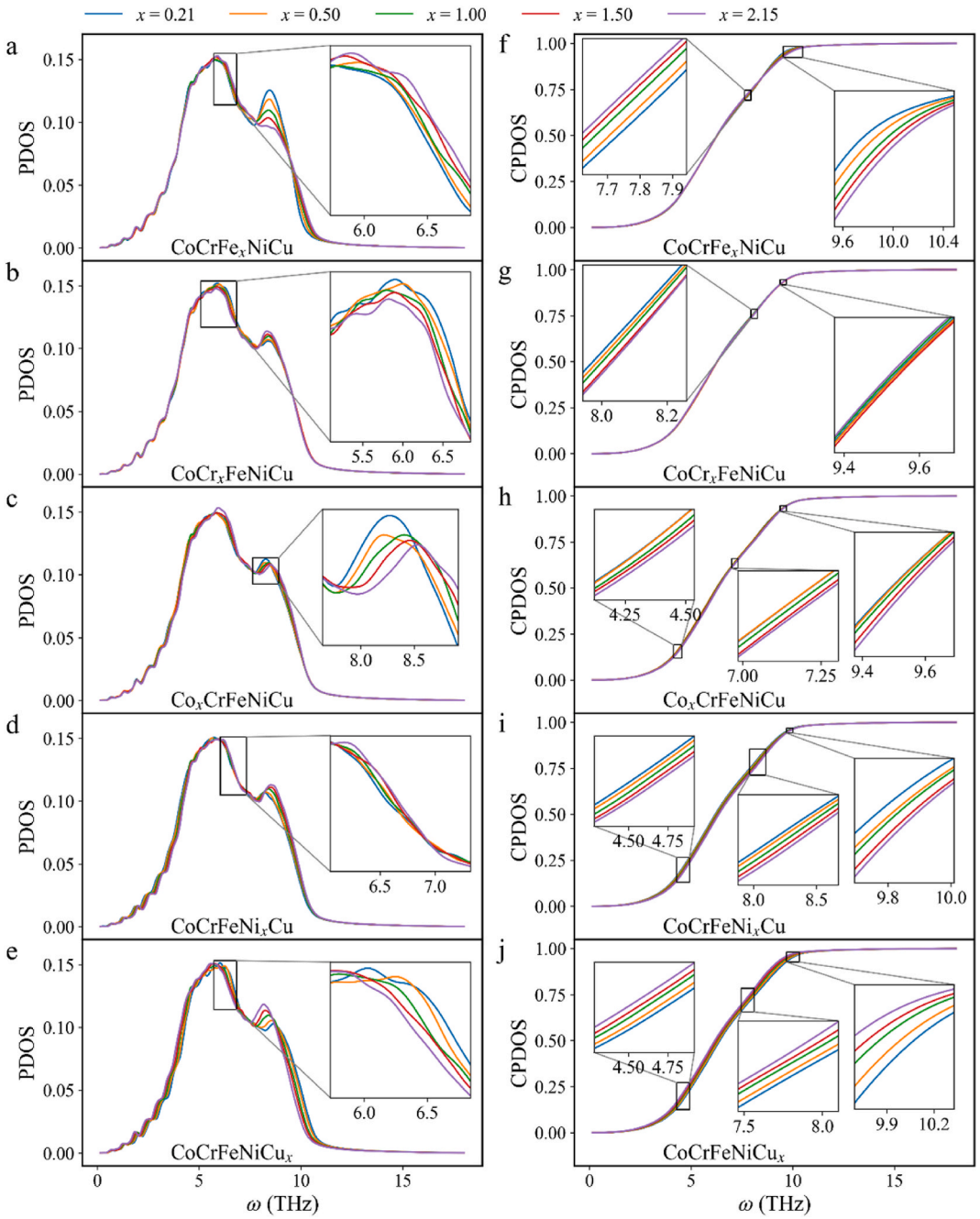

Fig. 7. PDOS and CPDOS of CoCrFeNiCu HEAs. a. PDOS of the CoCrFe$_x$NiCu HEA (x = 0.21, 0.5, 1, 1.5 and 2.15); b. PDOS of the CoCr$_x$FeNiCu HEA (x = 0.21, 0.5, 1, 1.5 and 2.15); c. PDOS of the Co$_x$CrFeNiCu HEA (x = 0.21, 0.5, 1, 1.5 and 2.15); d. PDOS of the CoCrFeNi$_x$Cu HEA (x = 0.21, 0.5, 1, 1.5 and 2.15); e. PDOS of the CoCrFeNiCu$_x$ HEA (x = 0.21, 0.5, 1, 1.5 and 2.15); f. CPDOS of the CoCrFe$_x$NiCu HEA (x = 0.21, 0.5, 1, 1.5 and 2.15); g. CPDOS of the CoCr$_x$FeNiCu HEA (x = 0.21, 0.5, 1, 1.5 and 2.15); h. CPDOS of the Co$_x$CrFeNiCu HEA (x = 0.21, 0.5, 1, 1.5 and 2.15); i. CPDOS of the CoCrFeNi$_x$Cu HEA (x = 0.21, 0.5, 1, 1.5 and 2.15); j. CPDOS of the CoCrFeNiCu$_x$ HEA (x = 0.21, 0.5, 1, 1.5 and 2.15).

cases, as high temperatures may induce the Umklapp scattering via which phonons are coupled to high frequency. When the temperature rises, the interatomic distance increases due to the energized atoms, leading to reduced phonon interactions and reduced phonon vibrations.

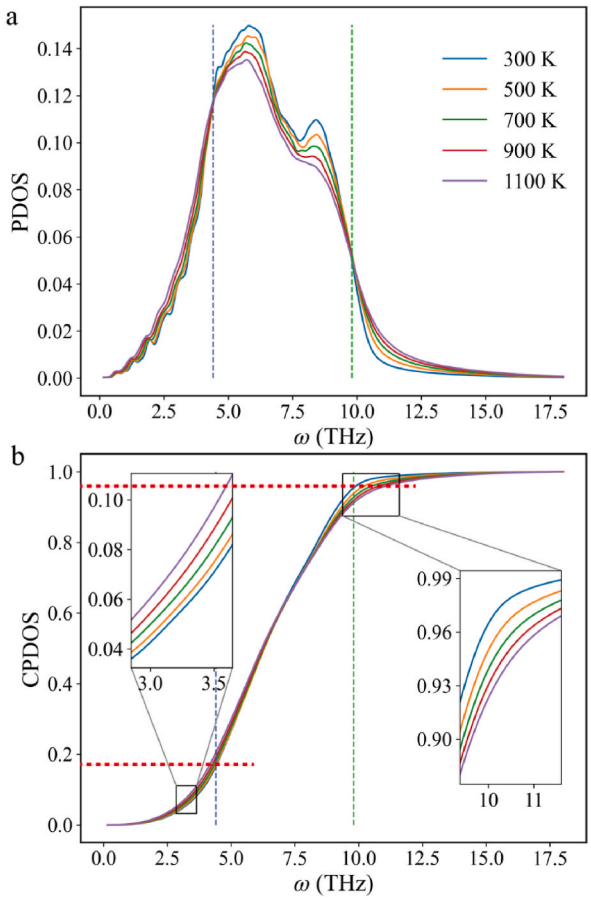

Fig. 8. The PDOS and CPDOS in the equiatomic CoCrFeNiCu HEA at different temperatures. a. PDOS. b.CPDOS.

3.4. Mean free path of phonons

To gain additional insights into the phonon behaviour in equiatomic CoCrFeNiCu HEA, the mean phonon velocity v, phonon mean free path (MFP) l_p, and lifetime of phonons τ at different temperatures were calculated. The mean phonon velocity, v, can be obtained from the slope of the $1/k_p$-$1/l_z$ fitting curve, l_p can be obtained from the expression $l_p = 3k_p/C_v v$, and the mean phonon lifetime τ equals l_p/v [52,53]. In Table 4, as the temperature increases from 300 K to 900 K, the phonon MFP is reduced by 46.5 %, the phonon velocity increases by 19.9 %. Such result shows that the phonon MFP is more sensitive to the temperature change. As the temperature increases, the atoms are accelerated and collisions are intensified. The accelerated thermal vibration of the lattice aggravates the lattice distortion [56] and thus increases the probability of the lattice defects, causing the scattering of phonons and reducing the MFP of phonons. At 300K, the phonon MFPs of pure metals Cu, Co, and Ni are approximately 100, 70, and 85 Å, respectively [57], which are much larger than the MFP of the equiatomic CoCrFeNiCu. This indicates that adding elements could significantly reduce the MFP of the alloy.

4. Conclusions

In this study, the thermophysical properties, including lattice thermal conductivity k_p and volumetric specific heat capacity C_v, of CoCrFeNiCu HEAs were investigated, for the first time, by a series of MD simulations. The effects of the atomic content of the comprising elements, the HEA size and the temperature on the k_p of nanoscale CoCrFeNiCu HEA were explored. The PDOS was used to reveal the underlying mechanism of the influence of element atomic contents and temperature on the conduction behaviours of HEAs from an atomic perspective.

The results show that k_p increases with the atomic contents of Co and Ni but decreases with Cu. The effects of atomic contents of Cr and Fe on the lattice thermal conductivity is insignificant. After eliminating the size effect of the equiatomic CoCrFeNiCu HEA, k_p and temperature T follows a power-law relationship with the order of temperature being -0.419 (i.e., $k_p \sim T^{-0.419}$). As the temperature increases, C_v of all HEAs slightly decreases and then increases. The PDOS analysis of the HEAs manifest that the phonons most vibrate at a frequency range less than 12.5 THz, which agrees with previous findings. For the equiatomic CoCrFeNiCu HEA, most of the phonons vibrate with a frequency between 4.4 THz and 9.8 THz. The number of phonons vibrating at such a range increases as

Table 4
Average velocity, mean free path and lifetime of phonons.

Temperature (K)	300	500	700	900	1100
v (km/s)	3.392	3.628	4.063	4.068	3.657
l_p (Å)	10.88	8.776	6.689	5.857	5.820
τ (ps)	0.321	0.242	0.165	0.139	0.162

temperature decreases, accounting for the decreasing trend of k_p with temperatures.

This study suggests a way to control the thermophysical properties of HEA by varying the atomic contents and provides theoretical foundations for material design of HEAs. In future research, DFT calculations can be conducted to gain additional insights into atomic behaviour. Also, the effects of external forces such as pressure and magnetic fields on the thermophysical properties of HEAs can be one direction for future research.

Data availability statement

Data will be made available on request.

CRediT authorship contribution statement

Fan Liu: Writing – original draft, Methodology, Data curation. **Yuqing Liu:** Writing – review & editing. **Xi Zhuo Jiang:** Writing – review & editing, Supervision, Funding acquisition, Conceptualization. **Jun Xia:** Writing – review & editing.

Declaration of competing interest

The authors declare that they have no known competing financial interests or personal relationships that could have appeared to influence the work reported in this paper.

Acknowledgement

This work was supported by the Liaoning Revitalization Talents Program (XLYC2203161) and the Starting Fund of Northeastern University, China.

Appendix A. Supplementary data

Supplementary data to this article can be found online at https://doi.org/10.1016/j.heliyon.2024.e36064.

References

[1] E.P. George, D. Raabe, R.O. Ritchie, High-entropy alloys, Nat. Rev. Mater. 4 (8) (2019) 515–534, https://doi.org/10.1038/s41578-019-0121-4.
[2] Z.T. Zhang, E. Axinte, W.J. Ge, C.Y. Shang, Y. Wang, Microstructure, mechanical properties and corrosion resistance of CuZrY/Al, Ti, Hf series high-entropy alloys, Mater. Des. 108 (2016) 106–113, https://doi.org/10.1016/j.matdes.2016.06.100.
[3] D.B. Miracle, O.N. Senkov, A critical review of high entropy alloys and related concepts, Acta Mater. 122 (2017) 448–511, https://doi.org/10.1016/j.actamat.2016.08.081.
[4] J.-W. Yeh, Alloy design strategies and future trends in high-entropy alloys, Jom 65 (12) (2013) 1759–1771, https://doi.org/10.1007/s11837-013-0761-6.
[5] M. Wang, Z.L. Ma, Z.Q. Xu, X.W. Cheng, y Microstructures and mechanical properties of HfNbTaTiZrW and HfNbTaTiZrMoW refractory high-entropy alloys, J. Alloys Compd. 803 (2019) 778–785, https://doi.org/10.1016/j.jallcom.2019.06.138.
[6] Z.F. Lei, X.J. Liu, Y. Wu, H. Wang, S.H. Jiang, S.D. Wang, X.D. Hui, Y.D. Wu, B. Gault, P. Kontis, D. Raabe, L. Gu, Q.H. Zhang, H.W. Chen, H.T. Wang, J.B. Liu, K. An, Q.S. Zeng, T.G. Nieh, Z.P. Lu, Enhanced strength and ductility in a high-entropy alloy via ordered oxygen complexes, Nature 563 (7732) (2018) 546, https://doi.org/10.1038/s41586-018-0685-y.
[7] J. Joseph, N. Haghdadi, M. Annasamy, S. Kada, P.D. Hodgson, M.R. Barnett, D.M. Fabijanic, On the enhanced wear resistance of CoCrFeMnNi high entropy alloy at intermediate temperature, Scripta Mater. 186 (2020) 230–235, https://doi.org/10.1016/j.scriptamat.2020.05.053.
[8] M. Loebel, T. Lindner, T. Mehner, T. Lampke, Influence of titanium on microstructure, phase formation and wear behaviour of AlCoCrFeNiTix high-entropy alloy, Entropy 20 (7) (2018), https://doi.org/10.3390/e20070505.
[9] H. Liu, J. Liu, X. Li, P.J. Chen, H.F. Yang, J.B. Hao, Effect of heat treatment on phase stability and wear behavior of laser clad AlCoCrFeNiTi0.8 high-entropy alloy coatings, Surf. Coating. Technol. 392 (2020), https://doi.org/10.1016/j.surfcoat.2020.125758.
[10] M.H. Chuang, M.H. Tsai, W.R. Wang, S.J. Lin, J.W. Yeh, Microstructure and wear behavior of AlxCo1.5CrFeNi1.5Tiy high-entropy alloys, Acta Mater. 59 (16) (2011) 6308–6317, https://doi.org/10.1016/j.actamat.2011.06.041.
[11] L. Huang, X.J. Wang, X.C. Zhao, C.Z. Wang, Y.S. Yang, Analysis on the key role in corrosion behavior of CoCrNiAlTi-based high entropy alloy, Mater. Chem. Phys. 259 (2021), https://doi.org/10.1016/j.matchemphys.2020.124007.
[12] J. Liu, H. Liu, P.J. Chen, J.B. Hao, Microstructural characterization and corrosion behaviour of AlCoCrFeNiTix high-entropy alloy coatings fabricated by laser cladding, Surf. Coating. Technol. 361 (2019) 63–74, https://doi.org/10.1016/j.surfcoat.2019.01.044.
[13] W.H. Guo, K.X. Zhang, Z.B. Liang, R.Q. Zou, Q. Xu, Electrochemical nitrogen fixation and utilization: theories, advanced catalyst materials and system design, Chem. Soc. Rev. 48 (24) (2019) 5658–5716, https://doi.org/10.1039/c9cs00159j.

[14] J. Gonzalez-Masis, J.M. Cubero-Sesin, A. Campos-Quiros, K. Edalati, Synthesis of biocompatible high-entropy alloy TiNbZrTaHf by high-pressure torsion, Materials Science and Engineering a-Structural Materials Properties Microstructure and Processing 825 (2021), https://doi.org/10.1016/j.msea.2021.141869.
[15] X.H. Yan, Y. Zhang, Functional properties and promising applications of high entropy alloys, Scripta Mater. 187 (2020) 188–193, https://doi.org/10.1016/j.scriptamat.2020.06.017.
[16] O.N. Senkov, G.B. Wilks, J.M. Scott, D.B. Miracle, Mechanical properties of Nb25Mo25Ta25W25 and V20Nb20Mo20Ta20W20 refractory high entropy alloys, Intermetallics 19 (5) (2011) 698–706, https://doi.org/10.1016/j.intermet.2011.01.004.
[17] A. Sharma, M.C. Oh, B. Ahn, Microstructural evolution and mechanical properties of non-Cantor AlCuSiZnFe lightweight high entropy alloy processed by advanced powder metallurgy, Materials Science and Engineering a-Structural Materials Properties Microstructure and Processing 797 (2020), https://doi.org/10.1016/j.msea.2020.140066.
[18] J.W. Yeh, S.K. Chen, S.J. Lin, J.Y. Gan, T.S. Chin, T.T. Shun, C.H. Tsau, S.Y. Chang, Nanostructured high-entropy alloys with multiple principal elements: novel alloy design concepts and outcomes, Adv. Eng. Mater. 6 (5) (2004) 299–303, https://doi.org/10.1002/adem.200300567.
[19] B. Cantor, I.T.H. Chang, P. Knight, A.J.B. Vincent, Microstructural development in equiatomic multicomponent alloys, Materials Science and Engineering a-Structural Materials Properties Microstructure and Processing 375 (2004) 213–218, https://doi.org/10.1016/j.msea.2003.10.257.
[20] M. Caro, L.K. Béland, G.D. Samolyuk, R.E. Stoller, A. Caro, Lattice thermal conductivity of multi-component alloys, J. Alloys Compd. 648 (2015) 408–413, https://doi.org/10.1016/j.jallcom.2015.06.035.
[21] C. Cheng, S.Y. Ma, S.Q. Wang, The role of phonon anharmonicity on the structural stability and phonon heat transport of CrFeCoNiCux high-entropy alloys at finite temperatures, J. Alloys Compd. 935 (2023), https://doi.org/10.1016/j.jallcom.2022.168003.
[22] P. Bag, Y.-C. Su, Y.-K. Kuo, Y.-C. Lai, S.-K. Wu, Physical properties of face-centered cubic structured high-entropy alloys: effects of NiCo, NiFe, and NiCoFe alloying with Mn, Cr, and Pd, Phys. Rev. Mater. 5 (8) (2021), https://doi.org/10.1103/PhysRevMaterials.5.085003.
[23] Y. Shi, Q. Shu, P.K. Liaw, M. Wang, C.-L. Teng, H. Zou, P. Wen, B. Xu, D. Wang, J. Wang, Effect of annealing on mechanical and thermoelectric properties of a Al2CoCrFeNi high-entropy alloy, Mater. Des. 213 (2022), https://doi.org/10.1016/j.matdes.2021.110313.
[24] S. Shafeie, S. Guo, Q. Hu, H. Fahlquist, P. Erhart, A. Palmqvist, High-entropy alloys as high-temperature thermoelectric materials, J. Appl. Phys. 118 (18) (2015), https://doi.org/10.1063/1.4935489.
[25] J. Yang, W. Ren, X. Zhao, T. Kikuchi, P. Miao, K. Nakajima, B. Li, Z. Zhang, Mictomagnetism and suppressed thermal conduction of the prototype high-entropy alloy CrMnFeCoNi, J. Mater. Sci. Technol. 99 (2022) 55–60, https://doi.org/10.1016/j.jmst.2021.04.077.
[26] H.-P. Chou, Y.-S. Chang, S.-K. Chen, J.-W. Yeh, Microstructure, thermophysical and electrical properties in AlxCoCrFeNi ($0 \leq x \leq 2$) high-entropy alloys, Mater. Sci. Eng., B 163 (3) (2009) 184–189, https://doi.org/10.1016/j.mseb.2009.05.024.
[27] K. Han, H. Jiang, T. Huang, M. Wei, Thermoelectric properties of CoCrFeNiNbx eutectic high entropy alloys, Crystals 10 (9) (2020), https://doi.org/10.3390/cryst10090762.
[28] I.H. Kim, H.S. Oh, K.S. Lee, E.S. Park, Optimization of conflicting properties via engineering compositional complexity in refractory high entropy alloys, Scripta Mater. 199 (2021), https://doi.org/10.1016/j.scriptamat.2021.113839.
[29] X.Z. Jiang, K.H. Luo, Y. Ventikos, Principal mode of Syndecan-4 mechanotransduction for the endothelial glycocalyx is a scissor-like dimer motion, Acta Physiol. 228 (3) (2020) e13376, https://doi.org/10.1111/apha.13376.
[30] C.Y. Zhao, Y.B. Tao, Y.S. Yu, Thermal conductivity enhancement of phase change material with charged nanoparticle: a molecular dynamics simulation, Energy 242 (2022), https://doi.org/10.1016/j.energy.2021.123033.
[31] X. Wu, Q. Han, Thermal transport in pristine and defective two-dimensional polyaniline (C3N), Int. J. Heat Mass Tran. 173 (2021), https://doi.org/10.1016/j.ijheatmasstransfer.2021.121235.
[32] S.F.M. Noraldeen, L. Jin, L. Zhou, Size, interface and temperature effects on specific heat capacities of Cu-water nanofluid and Cu nanoparticle: a molecular analysis, Therm. Sci. Eng. Prog. 27 (2022), https://doi.org/10.1016/j.tsep.2021.101157.
[33] H.F. Zhang, H.L. Yan, F. Fang, N. Jia, Orientation-Dependent mechanical responses and plastic deformation mechanisms of FeMnCoCrNi high-entropy alloy: a molecular dynamics study, Acta Metallurgica Sinica-English Letters 34 (11) (2021) 1511–1526, https://doi.org/10.1007/s40195-021-01260-y.
[34] X.Z. Jiang, Y. Ventikos, Molecular dynamics simulation: a new way to understand the functionality of the endothelial glycocalyx, Curr. Opin. Struct. Biol. 73 (2022) 102330, https://doi.org/10.1016/j.sbi.2022.102330.
[35] X.Z. Jiang, K.H. Luo, Y. Ventikos, Understanding the role of endothelial glycocalyx in mechanotransduction via computational simulation: a mini review, Front. Cell Dev. Biol. 9 (2021), https://doi.org/10.3389/fcell.2021.732815.
[36] X.Z. Jiang, K.H. Luo, Reactive and electron force field molecular dynamics simulations of electric field assisted ethanol oxidation reactions, Proc. Combust. Inst. 38 (4) (2021) 6605–6613, https://doi.org/10.1016/j.proci.2020.06.318.
[37] J. Wang, X.Z. Jiang, K.H. Luo, Exploring reaction mechanism for ammonia/methane combustion via reactive molecular dynamics simulations, Fuel 331 (2023) 125806, https://doi.org/10.1016/j.fuel.2022.125806.
[38] Z. Sun, C. Shi, L. Gao, S. Lin, W. Li, Thermal physical properties of high entropy alloy Al0.3CoCrFeNi at elevated temperatures, J. Alloys Compd. 901 (2022), https://doi.org/10.1016/j.jallcom.2021.163554.
[39] O.R. Deluigi, R.C. Pasianot, F.J. Valencia, A. Caro, D. Farkas, E.M. Bringa, Simulations of primary damage in a High Entropy Alloy: probing enhanced radiation resistance, Acta Mater. 213 (2021), https://doi.org/10.1016/j.actamat.2021.116951.
[40] B. Zhang, Y. Zhang, S.M. Guo, A thermodynamic study of corrosion behaviors for CoCrFeNi-based high-entropy alloys, J. Mater. Sci. 53 (20) (2018) 14729–14738, https://doi.org/10.1007/s10853-018-2652-2.
[41] J. Gao, Y. Jin, Y. Fan, D. Xu, L. Meng, C. Wang, Y. Yu, D. Zhang, F. Wang, Fabricating antibacterial CoCrCuFeNi high-entropy alloy via selective laser melting and in-situ alloying, J. Mater. Sci. Technol. 102 (2022) 159–165, https://doi.org/10.1016/j.jmst.2021.07.002.
[42] L. Chen, S.Y. Wang, W.Q. Tao, A study on thermodynamic and transport properties of carbon dioxide using molecular dynamics simulation, Energy 179 (2019) 1094–1102, https://doi.org/10.1016/j.energy.2019.05.073.
[43] D. Farkas, A. Caro, Model interatomic potentials and lattice strain in a high-entropy alloy, J. Mater. Res. 33 (19) (2018) 3218–3225, https://doi.org/10.1557/jmr.2018.245.
[44] W. Li, H. Fan, J. Tang, Q. Wang, X. Zhang, J.A. El-Awady, Effects of alloying on deformation twinning in high entropy alloys, Mater. Sci. Eng. 763 (2019) 138143, https://doi.org/10.1016/j.msea.2019.138143.
[45] H. Zhang, K.W. Siu, W. Liao, Q. Wang, Y. Yang, Y. Lu, In situ mechanical characterization of CoCrCuFeNi high-entropy alloy micro/nano-pillars for their size-dependent mechanical behavior, Mater. Res. Express 3 (9) (2016) 094002, https://doi.org/10.1088/2053-1591/3/9/094002.
[46] S. Huang, Á. Vida, A. Heczel, E. Holmström, L. Vitos, Thermal expansion, elastic and magnetic properties of FeCoNiCu-based high-entropy alloys using first-principle theory, J. Occup. Med. 69 (11) (2017) 2107–2112, https://doi.org/10.1007/s11837-017-2565-6.
[47] Y. Gu, L. Jiang, W. Jin, Z. Wei, X. Liu, M. Guo, K. Xia, L. Chen, Experimental research and molecular dynamics simulation on thermal properties of capric acid/ethylene-vinyl/graphene composite phase change materials, J. Ind. Eng. Chem. 99 (2021) 256–263, https://doi.org/10.1016/j.jiec.2021.04.039.
[48] A. Angayarkanni, V. Sunny, J. Philip, Effect of nanoparticle size, morphology and concentration on specific heat capacity and thermal conductivity of nanofluids, Journal of nanofluids 4 (2015) 302–309, https://doi.org/10.1166/jon.2015.1167.
[49] A. Islam, M.S. Islam, N. Ferdous, J. Park, A. Hashimoto, Vacancy-induced thermal transport in two-dimensional silicon carbide: a reverse non-equilibrium molecular dynamics study, Phys. Chem. Chem. Phys. 22 (24) (2020) 13592–13602, https://doi.org/10.1039/d0cp00990c.
[50] N.L. Okamoto, K. Yuge, K. Tanaka, H. Inui, E.P. George, Atomic displacement in the CrMnFeCoNi high-entropy alloy – a scaling factor to predict solid solution strengthening, AIP Adv. 6 (12) (2016), https://doi.org/10.1063/1.4971371.
[51] H. Wang, Q. He, X. Gao, Y. Shang, W. Zhu, W. Zhao, Z. Chen, H. Gong, Y. Yang, Multifunctional high entropy alloys enabled by severe lattice distortion, Adv. Mater. 36 (17) (2024) 2305453, https://doi.org/10.1002/adma.202305453.
[52] P.K. Schelling, S.R. Phillpot, P. Keblinski, Comparison of atomic-level simulation methods for computing thermal conductivity, Phys. Rev. B 65 (14) (2002), https://doi.org/10.1103/PhysRevB.65.144306.

[53] S. Stackhouse, L. Stixrude, B.B. Karki, Thermal conductivity of periclase (MgO) from first principles, Phys. Rev. Lett. 104 (20) (2010) 208501, https://doi.org/10.1103/PhysRevLett.104.208501.
[54] M.L. Ali, E. Haque, M.Z. Rahaman, Pressure- and temperature-dependent physical metallurgy in a face-centered cubic NiCoFeCrMn high entropy alloy and its subsystems, J. Alloys Compd. 873 (2021), https://doi.org/10.1016/j.jallcom.2021.159843.
[55] S. Namsani, S. Auluck, J.K. Singh, Thermal conductivity of thermoelectric material β-Cu2Se: implications on phonon thermal transport, Appl. Phys. Lett. 111 (16) (2017), https://doi.org/10.1063/1.4999405.
[56] B. Chen, S. Li, J. Ding, X. Ding, J. Sun, E. Ma, Correlating dislocation mobility with local lattice distortion in refractory multi-principal element alloys, Scripta Mater. 222 (2023) 115048, https://doi.org/10.1016/j.scriptamat.2022.115048.
[57] Z. Tong, S. Li, X. Ruan, H. Bao, Comprehensive first-principles analysis of phonon thermal conductivity and electron-phonon coupling in different metals, Phys. Rev. B 100 (14) (2019) 144306, https://doi.org/10.1103/PhysRevB.100.144306.